J. Fluid Mech. (1976), *vol.* 74, *part* 1, *pp.* 31–58
Printed in Great Britain

Numerical simulation of the transition from three- to two-dimensional turbulence under a uniform magnetic field

By U. SCHUMANN

Kernforschungszentrum Karlsruhe, Institut für Reaktorentwicklung
75 Karlsruhe, Postfach 3640, West Germany

(Received 12 September 1975)

The transition of homogeneous turbulence from an initially isotropic three-dimensional to a quasi-two-dimensional state is simulated numerically for a conducting, incompressible fluid under a uniform magnetic field $\mathbf{B}_0$. The magnetic Reynolds number is assumed to be small, so that the induced fluctuations of the magnetic field are small compared with the imposed magnetic field $\mathbf{B}_0$, and can be computed from a quasi-static approximation. If the imposed magnetic field is strong enough, all variations of the flow field in the direction of $\mathbf{B}_0$ are damped out. This effect is important e.g. in the design of liquid-metal cooling systems for fusion reactors, and the properties of the final state are relevant to atmospheric turbulence. An extended version of the code of Orszag & Patterson (1972) is used to integrate the Navier–Stokes equations for an incompressible fluid. The initial hydrodynamic Reynolds number is 60. The magnetic interaction number N is varied between zero and 50. Periodic boundary conditions are used. The resolution corresponds to 32^3 points in real space. The full nonlinear simulations are compared with otherwise identical linear simulations; the linear results agree with the nonlinear ones within 3 % for about one-fifth of the large-scale turnover time. This departure is a consequence of the return-to-equilibrium tendencies caused mainly by energy transfer towards high wavenumbers. The angular energy transfer and the energy exchange between different components are smaller, and become virtually zero for large values of N. For $N \approx 50$ we reach a quasi-two-dimensional state. Here, the energy transfer towards high wavenumbers is reduced for the velocity components perpendicular to $\mathbf{B}_0$ but relatively increased for the component parallel to $\mathbf{B}_0$. The overall behaviour is more similar to three- than to purely two-dimensional turbulence. This finding is of great importance for turbulence models of the atmosphere. The realization of a purely two-dimensional state does not seem to be possible for decaying turbulence. The magnetic field causes highly intensified pressure fluctuations, which contribute to the redistribution of the anisotropic Lorentz forcing.

1. Introduction

The impact of a strong uniform magnetic field on initially isotropic and homogeneous turbulence is studied by direct spectral simulation. The transition towards a two-dimensional state is investigated with special emphasis on the

effects of nonlinearities and pressure fluctuations. We consider a Newtonian incompressible fluid with constant density ρ, kinematic viscosity ν, and magnetic diffusivity η. The magnetic Reynolds number is

$$Rm_L \equiv vL/\eta. \tag{1}$$

v is the root-mean-square (r.m.s.) velocity, and L is the integral length scale (defined as the integral over the normalized longitudinal velocity correlation function: see e.g. Batchelor 1959). It is assumed that

$$Rm_L \ll 1. \tag{2}$$

Thus the fluctuations $\mathbf{b}$ around the mean (imposed) magnetic field $\mathbf{B}_0$ are small ($|\mathbf{b}| \ll |B_0|$), and can be computed from a quasi-static theory, deduced, e.g., by Roberts (1967, §§ 2.1, 5.4). In this case, the Lorentz force $\mathbf{F}$ induced by the magnetic field $\mathbf{B}$ becomes a linear function of the velocity field $\mathbf{u}$.

The numerical method is as developed by Orszag & Patterson (1972) and extended by Schumann & Patterson (1976*a*). The only change incorporated in the present scheme is the inclusion of the Lorentz force. The three-dimensional Navier–Stokes equations are solved numerically, using a Galerkin approximation based on a Fourier-spectral representation of the flow field $\mathbf{u}(\mathbf{x},t)$. ($\mathbf{x}$ is space position, t time.) Periodic boundary conditions are imposed on the sides of a cubic box of side length L_{box}, so that $\mathbf{u}(\mathbf{x},t)$ has the discrete Fourier representation

$$\mathbf{u}(\mathbf{x},t) = \sum_{\text{all } \mathbf{k}} \hat{\mathbf{u}}(\mathbf{k},t) \exp[i\,\mathbf{k}.\mathbf{x}], \quad i = \sqrt{-1}. \tag{3}$$

$\mathbf{k} = k_{\min}\mathbf{M}$ is the wavenumber vector, and $\mathbf{M}$ is a unit vector. The smallest non-zero wavenumber has the magnitude $k_{\min} = 2\pi/L_{\mathrm{box}}$. Only the modes $\hat{\mathbf{u}}(\mathbf{k},t)$ with $|\mathbf{k}| < k_{\max}$ are retained for the numerical procedure. In this study, $k_{\max}/k_{\min} = (242)^{\frac{1}{2}} \approx 15{\cdot}6$. This spectral truncation determines the maximum hydrodynamic Reynolds number

$$Re_L \equiv vL/\nu \tag{4}$$

that may be used for accurate simulations. The present numerical simulations are for $Re_L \approx 60$.

Assumption (2) is valid for most laboratory and technical flows, since the magnetic Prandtl number

$$Pm \equiv \nu/\eta = Rm_L/Re_L \tag{5}$$

is generally very small for liquid metals (e.g. $\approx 10^{-7}$ for mercury, and $\approx 10^{-5}$ for sodium: Roberts 1967). Without this assumption, the magnetic field would have to be determined simultaneously with the velocity field by integrating Maxwell's equations. This doubles the number of degrees of freedom, and introduces computational difficulties (e.g. reduced time steps owing to instabilities triggered by Alvén waves: Roberts 1967). Although such an approach is possible and has been carried out (for $Pm \approx 1$) by Pouquet & Patterson (1976), it would be inappropriate for small magnetic Reynolds numbers.

As discussed by Lehnert (1955), Moffatt (1967), Moreau (1968), Kit & Tsinober (1971) and others, a strong magnetic field with $Rm \ll 1$ tends to eliminate velocity

gradients in the direction of $\mathbf{n} \equiv \mathbf{B}_0/|B_0|$. This tendency eventually results in a final 'two-dimensional' state, where all variables are independent of the $\mathbf{n}$ co-ordinate. This effect is important e.g. in the design of liquid-metal cooling systems for fusion reactors. It results in reduced turbulent heat transfer and friction. It is assumed that this effect also permits the laboratory experimental study of large-scale atmospheric turbulence, which is believed to be best approximated by a two-dimensional turbulence theory. As yet, such theories (e.g. that of Leith 1968) can be checked in a conclusive manner only against numerical experiments such as those of Lilly (1971) and Herring *et al.* (1974).

However, the two-dimensional state can be reached only if the Lorentz force and the resulting damping are strong enough to overcome the inherent instability of the turbulent flow and the resultant energy transfer due to the inertial (nonlinear) terms. The latter tends to effect a return to the three-dimensional state, and thus to isotropy. (See e.g. Schumann & Patterson 1976*b*.) The ratio between the magnetic damping and the inertial terms is usually (Moffatt 1967) characterized by the interaction number

$$N = \sigma \mathbf{B}_0^2 L/(\rho v). \tag{6}$$

σ is the electrical conductivity

$$\sigma = 1/(\eta \mu_0), \tag{7}$$

and μ_0 is the magnetic permeability (Roberts 1967). It is expected that a critical value N_c exists such that for $N \geqslant N_c$ the Lorentz force is strong enough to push the flow completely into the two-dimensional state. Also, one would like to know the value $N_{\min}$ that N may not exceed if departures from isotropy are to be negligible. These two values can be determined only if the nonlinear terms are known.

In all previous studies the nonlinear terms have been neglected, excepting only qualitative considerations (Moffatt 1967; Moreau 1968). Furthermore, only a few experimental investigations are known (as e.g. that of Volkov 1973), and they suffer from inhomogeneities of the applied magnetic field and from the limited number of measurable quantities. It appears that the quantitative effects of the nonlinear terms are virtually unknown. Even their qualitative importance has not yet been conclusively demonstrated.

The present contribution describes the results of several 'numerical experiments'. Each one is a flow simulation starting from the same initial velocity field, which is Gaussian random, at time $t = 0$. During $0 \leqslant t < t_1$, we assume a zero magnetic field, so that triple correlations, and thus the dynamics of the turbulence (Batchelor 1959), may evolve. At time $t = t_1$, we 'switch on' the magnetic field $\mathbf{B}_0$. (For a discussion of whether this is possible in physics, see Moffatt 1967.) This field is kept constant during $t_1 \leqslant t < t_2$, and during this time we study the turbulence as influenced by the Lorentz force. Finally, during $t_2 \leqslant t \leqslant t_3$ the magnetic field is again zero, and we investigate the eventual return to isotropy. The individual experiments differ in the size of $\mathbf{B}_0$ during $t_1 \leqslant t < t_2$. In terms of N at $t = t_1$, we consider $N \approx 0$, 1, 5 and 50, and a few results for $N \approx 2$. We then repeat each run as before, except that all nonlinear terms in the Navier–Stokes equations are set to zero for $t \geqslant t_1$. These 'linear' results are

compared with the full 'nonlinear' cases, to check the validity of linearized theories.

In addition to the velocity statistics we consider the pressure fluctuations. Since the divergence of the Lorentz force is not generally zero, a pressure field $p_1(\mathbf{x}, t)$ is induced as well as the pressure field $p_2(\mathbf{x}, t)$, which is a consequence of the convective terms and the equation of continuity. For large N, the p_1 fluctuations can be much larger than those of p_2, and might cause mechanical problems for the surrounding container. Like the Lorentz force, the p_1 field is a linear function of the velocity field. It is therefore relatively simple to evaluate the pressure–strain correlation for this pressure. The pressure–strain correlation must be known if phenomenological turbulence models (see e.g. Reynolds 1973) are to be applied to this problem. With regard to the p_2 field, this correlation has been studied numerically by Schumann & Patterson (1976*b*) and Schumann & Herring (1976). We shall see, however, that the results of those studies are not applicable to the present problem, without change. A complete understanding of all physical aspects of the present problem for homogeneous turbulence is necessary before e.g. a channel flow can be attacked or turbulence models can be designed. It is possible that the latter would be unsuitable for modelling the total flow, but entirely acceptable as subgrid scale models (Schumann 1975) within direct numerical simulations of the energy-containing scales of the flow.

The present approach suffers from certain essential limitations, however. The main examples are statistical uncertainties (Schumann & Herring 1976), departure from isotropy in the initial state (Schumann & Patterson 1976*a*), and limited resolution in wavenumber space. The first two are of minor importance (since most results are of a comparative nature and all runs are started from identical initial conditions); and they would completely disappear if we were to take averages over several statistically equivalent runs. This possibility is virtually eliminated because of the long computing time needed for a single run (about 18 min on a Control Data 7600). The limited resolution is important. As stated above, the Reynolds number is limited by the high-wavenumber cut-off (unless we use subgridscale models). An inertial subrange (Batchelor 1959) does not exist for the value $Re_L \approx 60$. The low-wavenumber cut-off (a consequence of the limited box size L_{box}) also becomes important, especially if the state of the turbulence is 'nearly' two-dimensional, since we are unable to resolve the very long waves in the $\mathbf{n}$ direction (which are the least-damped). Also, the coarse and rectangular distribution of discrete wavenumber vectors limits the angular resolution, which becomes important for large departures from isotropy (Schumann & Herring 1976). With respect to resolution, the results are most accurate for small values of N.

2. The basic equations

The Navier–Stokes equations for the velocity field $\mathbf{u}(\mathbf{x}, t)$, including the Lorentz force $\mathbf{F}$ (per unit mass), are

$$\frac{\partial}{\partial t}\mathbf{u} = \mathbf{q} - \nabla p + \mathbf{F} + \nu\nabla^2\mathbf{u}, \quad \nabla.\mathbf{u} = 0 \qquad (8a,b)$$

(Batchelor 1959). Here,

$$p(\mathbf{x},t) = p_1(\mathbf{x},t) + p_2(\mathbf{x},t)$$

is the total kinematic static pressure, and

$$\mathbf{q} = -(\mathbf{u}.\nabla)\mathbf{u} \tag{8c}$$

is the inertial forces vector. The Lorentz force is

$$\mathbf{F} = (\sigma/\rho)(\mathbf{j}\times\mathbf{B}) \tag{9}$$

(Roberts 1967). From Ohm's law, the electric current $\mathbf{j}$ is

$$\mathbf{j} = \sigma(\mathbf{E}+\mathbf{u}\times\mathbf{B}) \tag{10}$$

(Roberts 1967). $\mathbf{E}$ is the electrical field. For $Rm \ll 1$, the magnetic diffusion is large compared with the convective and local changes of the magnetic field, and its fluctuations $\mathbf{b}(\mathbf{x},t)$ around the imposed value $\mathbf{B}_0$ are, therefore, small. In this case, Maxwell's non-relativistic equations reduce (Roberts 1967, §2.2) in a first approximation to

$$\mathbf{B}(\mathbf{x},t) \equiv \mathbf{B}_0 + \mathbf{b}(\mathbf{x},t) \approx \mathbf{B}_0, \tag{11}$$

$$\mathbf{0} = \nabla\times(\mathbf{u}\times\mathbf{B}_0) + \eta\nabla^2\mathbf{b}, \quad \nabla.\mathbf{b} = 0, \tag{12}$$

$$\mathbf{j} = \mu_0^{-1}\nabla\times\mathbf{b}, \quad \mathbf{E} = -\nabla\Phi. \tag{13),(14}$$

Φ is a single-valued electrostatic potential, which satisfies

$$\nabla^2\Phi = \nabla.(\mathbf{u}\times\mathbf{B}_0) \tag{15}$$

(as a consequence of (10)–(14)). We easily verify that (10)–(15), together with proper boundary conditions, determine $\mathbf{F}$ implicitly, and note that $\mathbf{F}$ is linear in $\mathbf{u}$.

With periodic boundary conditions and the Fourier transformation (3), we have in Fourier space

$$\frac{d}{dt}\hat{\mathbf{u}}(\mathbf{k},t) = \hat{\mathbf{q}} - i\mathbf{k}\hat{p} + \hat{\mathbf{F}} - \nu k^2\hat{\mathbf{u}}, \tag{16}$$

$$\mathbf{k}.\hat{\mathbf{u}}(\mathbf{k},t) = 0. \tag{17}$$

(All transformed quantities are denoted by a circumflex.) The nonlinear term $\hat{\mathbf{q}}(\mathbf{k}, t)$ is computed as in Schumann & Patterson (1976*a*). (A small change in the notation is introduced for convenience.) The transformed Lorentz force in wave-number space can be given explicitly:

$$\hat{\mathbf{F}} = -\frac{\sigma}{\rho}\frac{1}{k^2}[\mathbf{k}\times(\mathbf{k}\times(\hat{\mathbf{u}}\times\mathbf{B}_0))]\times\mathbf{B}_0. \tag{18}$$

In the following we assume

$$\mathbf{n} = \mathbf{B}_0/|\mathbf{B}_0| = (0,0,1),$$

so that, using (17), the components of $\hat{\mathbf{F}}$ are

$$\hat{\mathbf{F}} = -\frac{\sigma B_0^2}{\rho k^2}\{k_3^2\hat{u}_1 - k_1k_3\hat{u}_3, k_3^2\hat{u}_2 - k_2k_3\hat{u}_3, 0\}. \tag{19}$$

The pressure $\hat{p}$ is eliminated by twice taking the cross-product of $\mathbf{k}$ with $d\hat{\mathbf{u}}(\mathbf{k},t)/dt$. Using (17), after some algebra, we get

$$\frac{d}{dt}\hat{\mathbf{u}}(\mathbf{k},t) = -\frac{1}{k^2}[\mathbf{k}\times(\mathbf{k}\times\hat{\mathbf{q}}(\mathbf{k},t))] - \left[\nu + \frac{\sigma}{\rho}\frac{(\mathbf{B}_0.\mathbf{k})^2}{k^4}\right] k^2\hat{\mathbf{u}}(\mathbf{k},t). \tag{20}$$

This shows the known result that the magnetic field $\mathbf{B}_0$ increases the effective viscosity (Lehnert 1955; Moffatt 1967; Moreau 1968; Kit & Tsinober 1971). This increase is dependent on $\mathbf{k}$, however, and thus anisotropic. The enhanced effective viscosity causes increased damping. This means that energy is taken out of the velocity field and put into the magnetic field $\mathbf{b}$, where it is in turn dissipated in Joule heat. (Comparison of (18) or (19) with (20) shows that the physics would be different for a compressible fluid. The Lorentz force $\mathbf{F}$ does not influence the $\mathbf{n}$ component of the velocity directly. Rather, it does so by means of the pressure field p_1.) Taking the dot product of $\mathbf{k}$ and $d\hat{\mathbf{u}}/dt$ (equation (16)), using (17), (18) we get

$$\hat{p}_1(\mathbf{k},t) = -i\frac{\sigma}{\rho}\frac{(\mathbf{k}.\mathbf{B}_0)(\hat{\mathbf{u}}.\mathbf{B}_0)}{k^2}, \tag{21}$$

$$\hat{p}_2(\mathbf{k},t) = -i\frac{\mathbf{k}.\hat{\mathbf{q}}}{k^2}. \tag{22}$$

Turbulence is described most simply in terms of statistical mean values. The second-order ensemble mean moments of $\hat{\mathbf{u}}$ are

$$\hat{E}_{ij}(\mathbf{k},t) = \langle\hat{u}_i(\mathbf{k},t)\hat{u}_j(-\mathbf{k},t)\rangle.$$

They represent the Fourier transform of $\langle u_i(\mathbf{x},t)u_j(\mathbf{x}+\mathbf{r},t)\rangle$ with respect to the separation $\mathbf{r}$ (Batchelor 1959). From (16) we find

$$\frac{d}{dt}\hat{E}_{ij} = \hat{\Gamma}_{ij} + \hat{\Phi}_{ij} - \hat{\phi}_{ij} - \hat{\psi}_{ij} - \hat{\epsilon}_{ij}. \tag{23}$$

All correlations on the right-hand side are of the form

$$\langle\hat{z}_i(\mathbf{k},t)\hat{u}_j(-\mathbf{k},t) + \hat{z}_j(\mathbf{k},t)\hat{u}_i(-\mathbf{k},t)\rangle$$

with $$\hat{z}_i = \{\hat{q}_i, -ik_i\hat{p}_2, ik_i\hat{p}_1, -\hat{F}_i, \nu k^2\hat{u}_i\}$$

for $$\{\hat{\Gamma}_{ij}, \hat{\Phi}_{ij}, \hat{\phi}_{ij}, \hat{\psi}_{ij}, \hat{\epsilon}_{ij}\},$$

which we call inertial energy transfer, nonlinear pressure energy transfer, linear pressure energy transfer, forcing, and viscous dissipation, respectively. The total nonlinear energy transfer is $\hat{\Gamma}_{ji} = \hat{\Gamma}_{ij} + \hat{\Phi}_{ij}$, and the total effect of the magnetic field in an incompressible fluid is the 'magnetic' or Joule dissipation

$$\hat{\mu}_{ij}(\mathbf{k},t) = \hat{\phi}_{ij} + \hat{\psi}_{ij} = 2\frac{\sigma}{\rho}\frac{(\mathbf{B}_0.\mathbf{k})^2}{k^2}\hat{E}_{ij}(\mathbf{k},t), \tag{24}$$

which is non-negative for $i = j$. Later we shall report results for some of these quantities summed over spherical shells $(k - \frac{1}{2}k_{\min} \leqslant |\mathbf{k}| < k + \frac{1}{2}k_{\min})$. These terms are distinguished by the parameters $(\mathbf{k},t)$ or (k,t). Also, the values $i = j = n$ are used for components in the $\mathbf{n}$ direction and $i = j = p$ for any perpendicular

component. If we sum the terms appearing in (23) over all wavenumbers $\mathbf{k}$, we obtain the real space 'energy' tensor

$$E_{ij}(t) = \langle u_i(\mathbf{x},t)u_j(\mathbf{x},t)\rangle$$

and similarly the viscous and magnetic dissipation tensors ϵ_{ij} and μ_{ij} and others. Using the summation convention for repeated subscripts i, j and k, but *not* for p or n, further definitions are

$$\left.\begin{aligned} &E = \tfrac{1}{2}E_{ii}, \quad \epsilon = \tfrac{1}{2}\epsilon_{ii}, \quad \mu = \tfrac{1}{2}\mu_{ii},\\ &v = (2E/3)^{\frac{1}{2}}, \quad L = \pi/(2v^2)\,\Sigma\,\hat{E}(\mathbf{k},t)/k,\\ &\lambda = [15\nu v^2/\epsilon]^{\frac{1}{2}}, \quad Re_\lambda = v\lambda/\nu,\\ &S = \tfrac{1}{35}[15\nu/\epsilon]^{\frac{3}{2}}\,\Sigma\,k^2\hat{\Gamma}_{ii}(\mathbf{k},t),\\ &C' = -\Phi_{23}L/(E^{\frac{1}{2}}\Delta E), \quad \Delta E = \tfrac{1}{3}(2E_{33}-E_{11}-E_{22}). \end{aligned}\right\} \tag{25}$$

These quantities we call the total energy, and the total viscous and magnetic dissipation; r.m.s. velocity and integral length scale; Taylor microscale and Taylor-scale Reynolds numbers; skewness; and Rotta's (1951) return-to-isotropy rate C', and energy difference. The summations Σ are over all wavenumbers $\mathbf{k}$ retained in the model.

3. Kinematics of the magnetic dissipation

In this section we present results that are consequences of the assumed initial isotropy and incompressibility. We discuss the evolution of the energy spectrum and the linear pressure fluctuations, neglecting nonlinear terms. With respect to the former, the essence of this linearized theory is not new (Lehnert 1955; Moffatt 1967; Moreau 1968; Kit & Tsinober 1971), but it is of great importance in interpreting the results. In particular, we stress that the magnetic dissipation causes not only an angular anisotropy, but also differences in the spherically integrated energies $\hat{E}_{ij}(\mathbf{k},t)$. (Here, we assume a continuous energy distribution in wavenumber space.) For isotropic turbulence we have

$$\hat{E}_{ij}(\mathbf{k},t) = U(k,t)\left(\delta_{ij}-\frac{k_ik_j}{k^2}\right), \quad U(k,t) \equiv \frac{\hat{E}(k,t)}{4\pi k^2} \tag{26}$$

(Batchelor 1959). Let $\mathbf{k} = \{k_1, k_2, k_3\}$ be expressed in spherical co-ordinates

$$\mathbf{k} = \{\sin\theta\sin\phi,\ \sin\theta\cos\phi,\ \cos\theta\}k. \tag{27a}$$

ϕ is the azimuthal angle around $\mathbf{n}$; and θ represents the angle between $\mathbf{n}$ and $\mathbf{k}$, so that

$$\cos\theta = \mathbf{k}.\mathbf{n}/|\mathbf{k}|. \tag{27b}$$

Then, we have

$$\hat{E}_{nn}(\mathbf{k},t) \equiv \hat{E}_{33}(\mathbf{k},t) = U(k,t)\sin^2\theta, \tag{28a}$$

$$\hat{E}_{pp}(\mathbf{k},t) \equiv \tfrac{1}{2}(\hat{E}_{11}(\mathbf{k},t)+\hat{E}_{22}(\mathbf{k},t)) = U(k,t)\,(\tfrac{1}{2}+\tfrac{1}{2}\cos^2\theta). \tag{28b}$$

This angular distribution is depicted in figure 1, which is a polar plot; it can also be interpreted as the plot of iso-energy lines (contours) if we assume $U(k) \sim k^{-1}$.

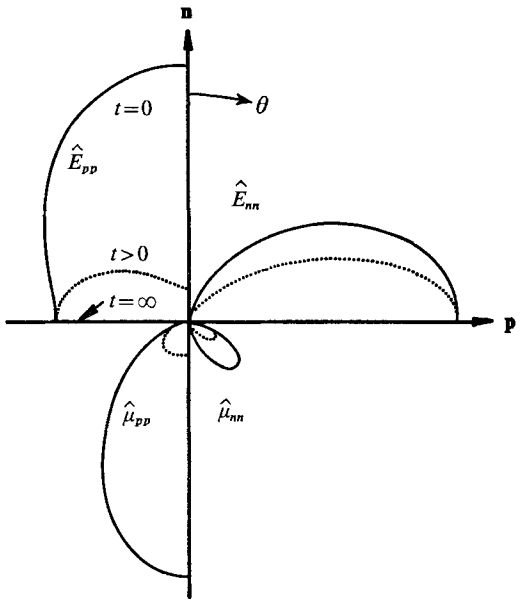

FIGURE 1. Schematic polar plot of the angular distribution of energy $\hat{E}$ and magnetic dissipation $\hat{\mu}$ in a plane containing the axis **n** of symmetry for the isotropic initial state and at later times. The distributions are mirror-symmetric with respect to **n** and **p** (any axis perpendicular to **n**).

The form of the contours (and, thus, any statement about the angle of that region which contains more than, say, the average magnetic dissipation: Moreau 1968) changes if we change the assumed function $U(k)$. The vanishing value of $\hat{E}_{nn}$ near **n** is a consequence of the fact that $\mathbf{k}.\hat{\mathbf{u}} = k_n \hat{u}_n = 0$ for $\mathbf{k} = \mathbf{n}$, but $k > 0$.

The magnetic dissipation $\hat{\mu}_{ij}$ is proportional to $\hat{E}_{ij}\cos^2\theta$, and its angular distribution (as shown in the lower part of figure 1) is therefore different for $i = j = n$ and $i = j = p$. Neglecting other contributions to $\partial\hat{E}_{ij}/\partial t$, this magnetic dissipation causes a reduction of $\hat{E}_{ij}$, so that after some time

$$\hat{E}_{ij}(\mathbf{k},t) = U(k,0)\left(\delta_{ij} - \frac{k_i k_j}{k^2}\right)\exp\left[-2\frac{\sigma}{\rho}B_0^2 t\cos^2\theta\right]. \tag{29}$$

Such an evolution for finite values of t is illustrated in figure 1 by the dotted curves. We see that energy is dissipated mainly near the axis **n** and more for $\hat{E}_{pp}$ than $\hat{E}_{nn}$. The turbulence is no longer isotropic rather than axisymmetric with respect to the axis of symmetry **n**. For $t \to \infty$, the energy is totally dissipated everywhere except for $\theta = 90°$. In this state, the remaining flow field is independent of the **n** co-ordinate and, therefore, we have a two-dimensional state. This effect is best illustrated by the mean-square velocity gradients in **n** direction

$$\left\langle \frac{\partial u_i}{\partial x_n}\frac{\partial u_j}{\partial x_n}\right\rangle = \iiint k_n^2 E_{ij}(\mathbf{k})\,d\mathbf{k} \to 0. \tag{30}$$

These, and similarly the pressure gradients $\langle(\partial p/\partial x_n)^2\rangle$, approach zero. We note, however, this does not imply that the velocity component in the **n** direction is zero. On the contrary, we find, for the spherical integrals,

$$\hat{E}_{nn}(k,\infty)/\hat{E}_{pp}(k,\infty) = 2. \tag{31}$$

The Lorentz force (see (19)), the induced linear pressure fluctuations p_1, and the magnetic dissipation would also go to zero.

This elimination of the magnetic dissipation, however, raises the question of whether this two-dimensional state can really be reached, since this requires that the nonlinear terms go to zero faster than the magnetic dissipation. It may be that we attain only a 'quasi-two-dimensional' state (Kit & Tsinober 1971), where all gradients in the **n** direction are sufficiently small only with respect to some *ad hoc* measure.

For any, say $\hat{X}_{ij}(\mathbf{k},t)$, of those tensors appearing in (23), we obtain the spherical integral from

$$\hat{X}_{ij}(k,t) = k^2\int_{\phi=0}^{2\pi}\int_{\theta=0}^{\pi}\hat{X}_{ij}(\mathbf{k},t)\sin\theta\, d\theta\, d\phi, \tag{32}$$

with **k** as given in (27) (Batchelor 1959). This integration results for the initial isotropic state in

$$\hat{\mu}_{ij}(k) = (8,8,4)\tfrac{1}{15}\hat{E}(k)\sigma B_0^2/\rho, \tag{33}$$

$$\hat{\psi}_{ij}(k) = (10,10,0)\tfrac{1}{15}\hat{E}(k)\sigma B_0^2/\rho, \tag{34}$$

$$\hat{\phi}_{ij}(k) = (-2,-2,4)\tfrac{1}{15}\hat{E}(k)\sigma B_0^2/\rho. \tag{35}$$

Here, the bracketed values correspond to the diagonal components

$$i = j = (1,2,3),$$

respectively; the off-diagonal components are zero. Equation (35) can be expressed in the generalized form

$$\hat{\phi}_{ij}(k) = -C_F(\hat{\psi}_{ij}(k) - \tfrac{1}{3}\delta_{ij}\,\hat{\psi}_{kk}(k)), \tag{36}$$

with

$$C_F = 3\hat{\phi}_{nn}(k)/\hat{\psi}_{kk}(k) = \tfrac{3}{5}. \tag{37}$$

Equations (36), (37) are equally valid for the integrals over all wavenumbers, ϕ_{ij} and ψ_{ij}. The form of (36) is the same as that proposed for other types of pressure–strain correlations (as for the pressure fluctuations induced by shear or buoyancy: see e.g. Launder 1975). Equations (36), (37) might therefore be at least approximately valid for cases where $Rm \approx 1$ and for small deviations from isotropy. In fact, if $Rm \ll 1$ and the resultant anisotropy is as described by (29), for the limit $(\sigma/\rho)B_0^2 t \to \infty$ we find a value $C_F = \frac{1}{2}$. This deviation from the result (37) is of minor importance, since the magnitude of the $\hat{\psi}_{ij}(k)$ goes to zero in the same limit. The spectrum

$$\hat{P}_1^2(\mathbf{k},t) \equiv \langle\hat{p}_1(\mathbf{k},t)\hat{p}_1(-\mathbf{k},t)\rangle \tag{38}$$

is

$$\hat{P}_1^2(\mathbf{k},t) = \left(\frac{\sigma}{\rho}B_0^2\right)^2\frac{\hat{E}(k,t)}{4\pi k^2}\sin^2\theta\cos^2\theta, \tag{39}$$

so that

$$\hat{P}_1^2(k,t) = \frac{2}{15}\left(\frac{\sigma B_0^2}{\rho}\right)^2\frac{\hat{E}(k,t)}{k^2}. \tag{40}$$

An energy spectrum appropriate (Schumann & Patterson 1976*a*) for moderate hydrodynamic Reynolds numbers is

$$\hat{E}(k,t) = 16(2/\pi)^{\frac{1}{2}}v^2(t)k_p^{-5}k^4\exp[-2(k/k_p)^2]. \tag{41}$$

k_p is the wavenumber for which $\hat{E}(k,t)$ takes its maximum ('peak'). From this spectrum we find, after integration over all k, for the integral length scale defined in (25),

$$L = (2\pi)^{\frac{1}{2}}/k_p; \tag{42}$$

for the r.m.s. pressure (p_1) fluctuations,

$$P_1 = \left(\frac{2}{15\pi}\right)^{\frac{1}{2}}\frac{\sigma B_0^2 vL}{\rho}; \tag{43}$$

for the total magnetic dissipation,

$$\mu = (\sigma/\rho)B_0^2v^2; \tag{44}$$

for the total viscous dissipation,

$$\epsilon = \frac{15\pi}{2}\nu\frac{v^2}{L^2}; \tag{45}$$

and thus for μ/ϵ, a ratio which has the form of the square of the Hartmann number Ha,

$$Ha^2 \equiv \frac{\mu}{\epsilon} = \frac{2}{15\pi}\frac{\sigma B_0^2 L^2}{\rho\nu}. \tag{46}$$

The result (44) is independent of the shape of the energy spectrum $\hat{E}(k)$. The values of P_1, μ and Ha approach zero for large values of $(\sigma/\rho)B_0^2t$ in the linear approximation.

4. Numerical experiments

4.1. *Specification*

The general 'experimental' procedure was described in § 1. The method integrates (20). The initial condition is a realization of a random Gaussian velocity field with an energy spectrum as given in (41). The parameter k_p is chosen such that

$$k_p/k_{\min} = 3, \quad \text{i.e.} \quad L_{\text{box}}/L = 3(2\pi)^{\frac{1}{2}},$$

and

$$k_{\max}/k_p = 5{\cdot}185.$$

This value of k_p is larger by a factor of 1·26 than that used by Orszag & Patterson (1972) to enhance the resolution of the energy-containing region and to reduce statistical uncertainties. (The latter are large if the energy-containing region is resolved with too few wavenumbers.) It is, however, smaller than the k_p value used by Schumann & Herring (1976) to reach a higher Reynolds number. The initial value of $v_0 \equiv v(0)$ is set arbitrarily at $v_0 = 1$. The time integration is done in finite time steps $\Delta t = 0{\cdot}02/(v_0 k_{\min})$. The nonlinear terms are treated by the second-order leapfrog method, together with a first-order Euler step (see Lilly 1965) every twentieth time step, to suppress numerical oscillations. The linear terms are accounted for by a factor

$$\exp[-(\nu k^2 + (\sigma/\rho)B_0^2\cos^2\theta)\Delta t];$$

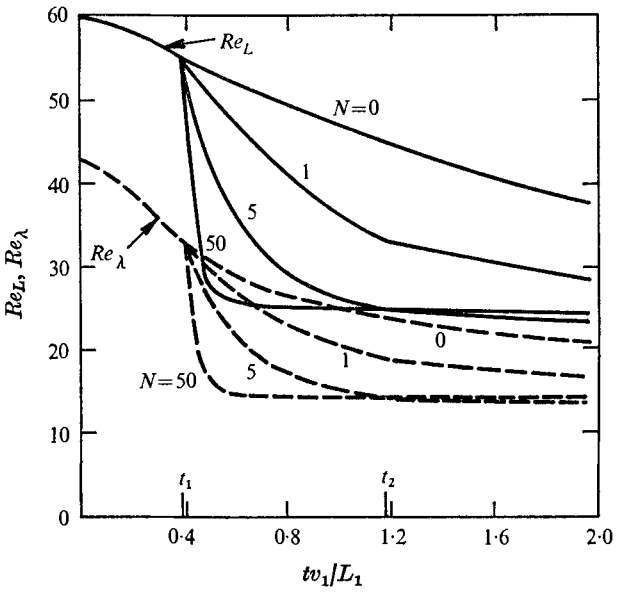

FIGURE 2. Integral-length-scale Reynolds number Re_L (——) and Taylor-scale Reynolds number Re_λ (– – – –) against normalized time for different values of the magnetic interaction number N. The magnetic field is zero outside $t_1 \leqslant t < t_2$.

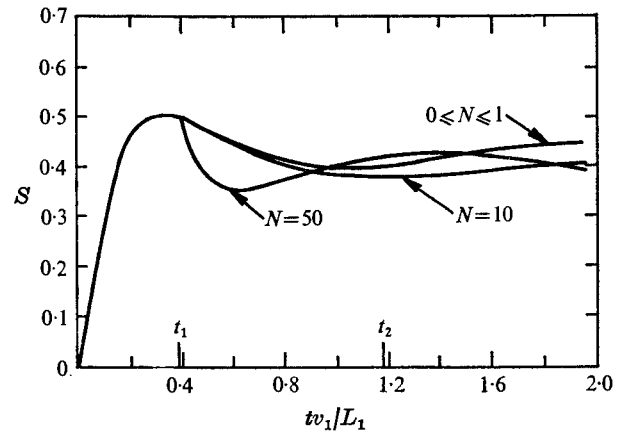

FIGURE 3. Skewness coefficient S against time for different values of the magnetic interaction number N.

this gives exact results if the nonlinear terms are absent. The viscosity ν is chosen to be $\nu = 0{\cdot}016\, v_0/k_{\min}$, which implies initial Reynolds numbers $Re_L = 59{\cdot}7$ and $Re_\lambda = 43{\cdot}0$. The time behaviour of both is plotted in figure 2. The first 20 time steps ($0 \leqslant t < t_1$) are integrated with zero magnetic field. During this time, the nonlinear energy transfer evolves as measured by the skewness factor S. (See figure 3.) It appears from the simulations that

$$L(0)/L(t_1) = 1{\cdot}002 \quad \text{and} \quad v(0)/v(t_1) = 1{\cdot}082.$$

In the following, all results are scaled with

$$L_1 \equiv L(t_1) \quad \text{and} \quad v_1 \equiv v(t_1).$$

The integral length scale L is taken instead of the more common Taylor microscale λ, since the magnetic dissipation is controlled by the energy-containing region. In these units, the times at which the magnetic field is switched on (t_1) or off (t_2), and where the computations are terminated (t_3), are

$$(t_1, t_2, t_3) = (0{\cdot}392, 1{\cdot}176, 1{\cdot}961) L_1/v_1.$$

During the time interval (t_1, t_2) the value of $\sigma B_0^2/\rho$ is set to (0, 1, 2, 5, or 50) $v_0 k_{\min}$, which results in rounded values (0, 1, 2, 5, or 50) for the interaction number N as defined in (6) and computed with $L = L_1$ and $v = v_1$. All cases are run twice, first with the full nonlinear method, and again with the linear part only ($\hat{\mathbf{q}} \equiv 0$ in (20)). In most of the following figures, nonlinear results are presented by solid and linear results by dashed curves.

4.2. *Verification of linear effects and implication of finite resolution*

Figures 4–10 illustrate the influence of the magnetic field, which is, in a first approximation, as expected from linear theories. (See § 3.)

The magnetic field initially increases the energy dissipation. This increase is apparent from the change in slope at $t = t_1$ in the energy ratio $E(t)/E(t_1)$ plotted in figure 4. The magnetic dissipation is plotted in figure 5. (In figures 5, 7, 8 and 16, we give the magnetic dissipation outside (t_1, t_2) *as if* the magnetic field were present at all times.) Figure 6 shows the viscous dissipation $\epsilon(t)/\epsilon(t_1)$; and figure 7 shows the ratio

$$Ha^2(t) = \mu(t)/\epsilon(t).$$

We notice the sharp reduction of magnetic dissipation at large values of N, which is a consequence of the large initial energy dissipation in the region near $\theta = 0°$, where most of the magnetic dissipation occurs. The region near $\theta = 90°$ is less affected and the decrease in $E(t)$ and $\epsilon(t)$ is thus smaller. For large values of Ntv_1/L_1, the turbulence becomes insensitive to the magnetic field. In figure 4 we see that the cusp at time $t = t_2$, which signals the eliminated magnetic dissipation, disappears for large values of N. Consequently, the Hartmann number decreases, as shown in figure 7. Figure 8 shows the ratio

$$Ha^2(k, t) \equiv \hat{\mu}(k, t)/\hat{\epsilon}(k, t)$$

against time and wavenumber k. The magnetic dissipation dominates at low wavenumbers, whereas the viscous dissipation becomes more important at high wavenumbers. The decrease of $Ha^2(k, t)$ against time is, within the linear approximation, independent of k.

The strong initial magnetic dissipation near $\theta = 0°$ results in the transition to the two-dimensional state. The transition is evident in figure 9, which shows the mean-square velocity gradient of the u_p component in the $\mathbf{n}$ direction. This value is normalized so that it is unity for isotropic turbulence. The initial departure from

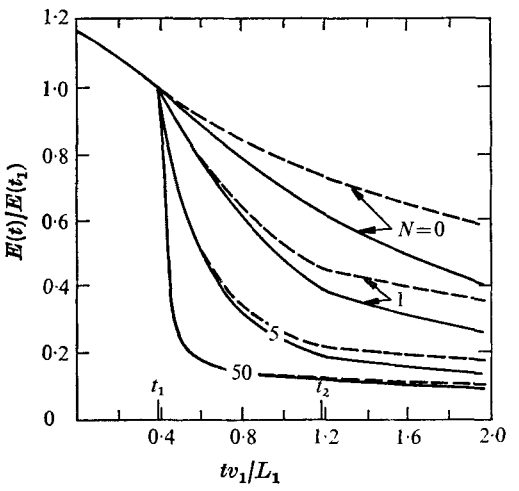

FIGURE 4

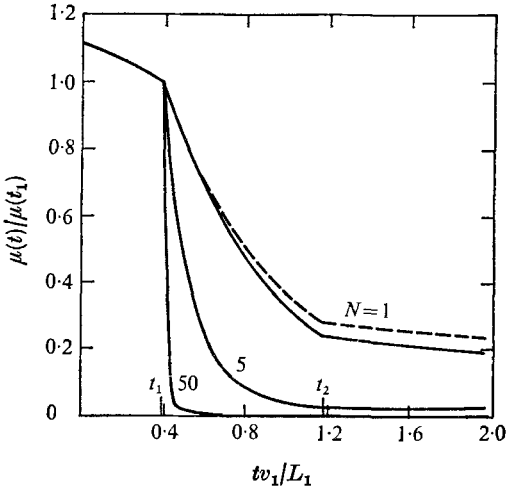

FIGURE 5

FIGURE 4. Normalized energy against time for different values of N. ——, results of the nonlinear simulations; – – –, those of the linear simulations.

FIGURE 5. Magnetic dissipation against time. Curves as in figure 4. The results are plotted as if the magnetic field would be constant at all times. Linear and nonlinear results are not distinguishable for $N \geqslant 5$.

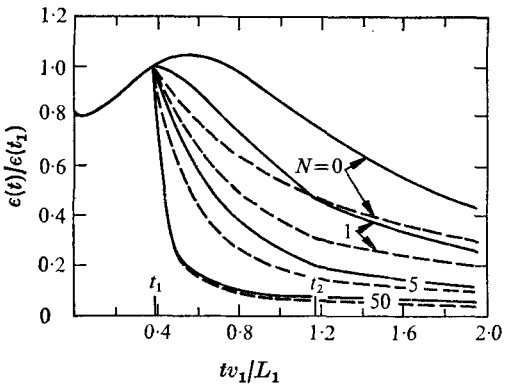

FIGURE 6

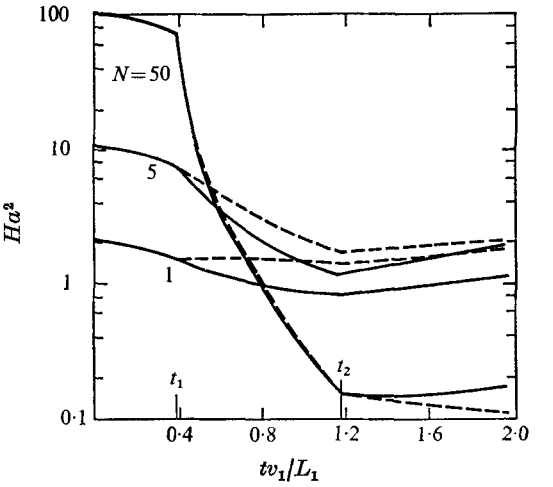

FIGURE 7

FIGURE 6. Viscous dissipation against time. Curves as in figure 4.

FIGURE 7. $Ha^2 = \mu/\epsilon$ against time. Curves as in figure 4. The magnetic field is assumed to be as in figure 5.

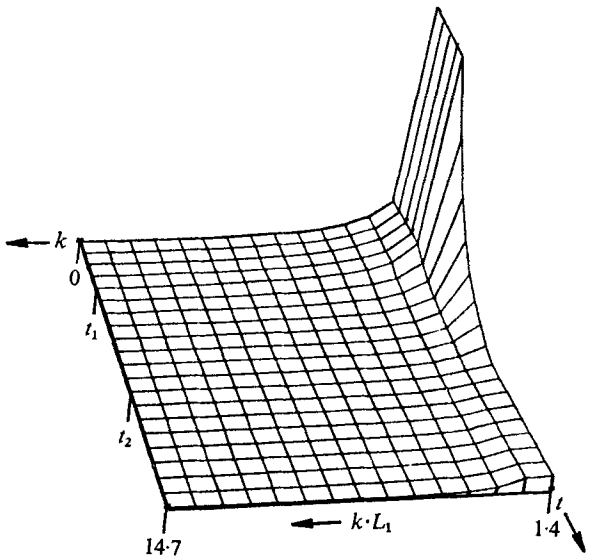

FIGURE 8. Squared Hartmann number against wavenumber k and time t:

$$Ha^2(k, t) = \hat{\mu}(k, t)/\hat{e}(k, t).$$

$N = 5$. The magnetic field is as in figure 5. The values of Ha^2 at $kL_1 = (1{\cdot}4, 14{\cdot}7)$ are $Ha^2(t = t_1) = (96{\cdot}4, 0{\cdot}474)$ and $Ha^2(t = t_2) = (5{\cdot}92, 0{\cdot}219)$, respectively.

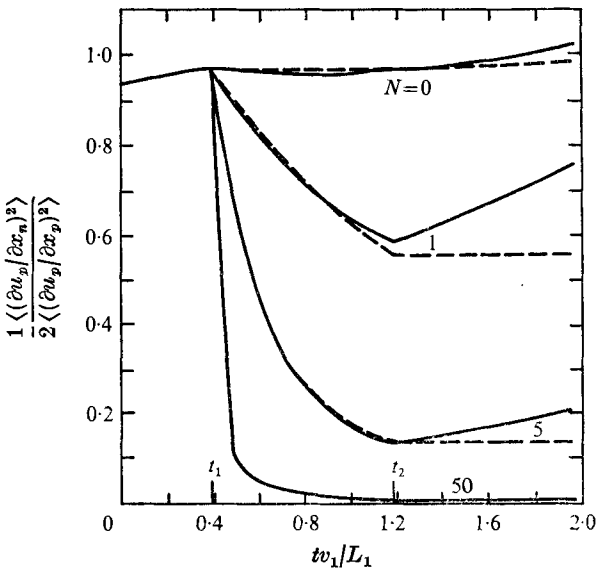

FIGURE 9. Normalized mean-square velocity gradient against time.
Curves as in figure 4.

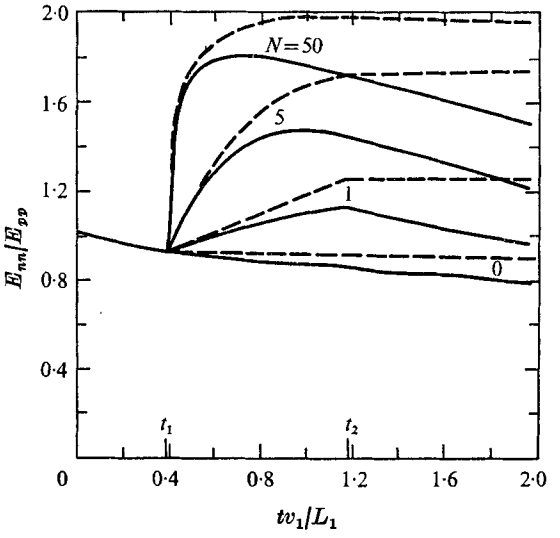

FIGURE 10. Ratio E_{nn}/E_{pp} against time. Curves as in figure 4.

unity is a consequence of the incomplete isotropy of the initial state. The tendency towards zero increases with N. Similar results have been found for

$$2\langle(\partial u_n/\partial x_n)^2\rangle/\langle(\partial u_n/\partial x_p)^2\rangle \quad \text{and for} \quad \cdot\langle(\partial p_2/\partial x_n)^2\rangle/\langle\partial p_2/\partial x_p)^2\rangle,$$

but the tendency towards zero is strongest for the ratio plotted in figure 9. The weaker decrease of $\langle(\partial u_n/\partial x_n)^2\rangle$ is a consequence of the relatively small values of $\hat{E}_{nn}(\mathbf{k})$ near $\theta = 0°$. (See figure 1.)

As predicted by the linear approximation, the ratio E_{nn}/E_{pp} grows when the magnetic field is increased. (See figure 10.) For large values of Ntv_1/L, this ratio approaches the theoretical limit 2 as given by (31), at least if we neglect the nonlinear effects.

Although the numerical procedure integrates the linearized equation (20) exactly, the result is not the exact solution for the physical problem, even if the equation could be linearized with impunity. This is because we use periodic boundary conditions on the sides of a cubic box of side length L_{box}, where L_{box} has a constant finite value. Accordingly we have only a discrete set of points in wavenumber space, whereas we would need a continuous spectrum to describe an infinite domain. In the simulations, the energy per mode represents the energy per volume $k_{\min}^3$ in wavenumber space, whereas in the continuum the energy is per infinitesimal volume $d\mathbf{k}$. As a consequence of the finite resolution, the energy in the region

$$\{-k_{\max} \leqslant k_1 < k_{\max}; \quad -k_{\max} \leqslant k_2 < k_{\max}; \quad -\tfrac{1}{2}k_{\min} \leqslant k_3 < \tfrac{1}{2}k_{\min}\}$$

is not affected directly by the magnetic dissipation. Therefore, if we neglect viscous dissipation and nonlinear energy transport, we never reach zero energy E. In fact, for large values of N we would finally reach a value that can be estimated from (41) to be

$$E(\infty)/E(0) \approx \tfrac{2}{3}(2/\pi)^{\frac{1}{2}}k_{\min}/k_p. \tag{47}$$

This has the value 0·177 in the present simulation. This value corresponds to the resultant value $E(t)/E(t_1)$ found in figure 4 for $N = 50$ at that time when the largest change in slope appears ($t \gtrapprox t_1$).

Note that the idea of an infinite domain is irrelevant for practical problems. Even so, one should keep in mind that, for the present problem, we get zero measurable velocity fluctuations at the same time as we reach the two-dimensional state exactly. We must therefore be content with the quasi-two-dimensional state.

Another implication of the periodic boundary conditions is that the angle between the plane $\mathbf{k}.\mathbf{n} = 0$ and the adjacent modes at $(k_1, k_2, k_{\min})$ is large for small values of $k_1^2 + k_2^2$. In fact, it is 18·4° for $k = k_p$ but 3·7° for $k = k_{\max}$. This means that the magnetic dissipation includes a larger angular region at high wavenumbers than at low ones, which distorts the results slightly.

Both resolution problems are of minor importance for small values of N. The present results suggest that the accuracy is sufficient at least for $N \leqslant 5$, and for the time intervals considered here.

4.3. *Nonlinear effects*

In three-dimensional turbulence, the nonlinear inertial and pressure forces produce an energy exchange between the different Fourier modes, until an isotropic equilibrium state is reached, where $\hat{E}_{ij}(\mathbf{k}, t)$ assumes the same value for all $\mathbf{k}$ and $i = j$. This is therefore also called the equi-partition state. In it, the energy spectrum is $\hat{E}(k) \sim k^2$. In reality, we never reach this spectrum, because of viscous dissipation at high wavenumbers. However, for model turbulence in a system with zero viscosity and with a finite truncation wavenumber $k_{\max}$, this spectrum was found by e.g. Orszag & Patterson (1972). The departure from the equilibrium state at high wavenumbers, to smaller energies, causes inertial energy transfer from low to high wavenumbers, as measured by $\hat{T}(k) = \frac{1}{2}\hat{\Gamma}_{ii}(k)$. This transfer function becomes negative at low and positive at high wavenumbers, while its integral is zero, since the inertial transfer is energy-conserving. This shape implies positive values of the skewness S, defined in (25) and depicted in figure 3. Special considerations are necessary for two-dimensional turbulence. (See below.)

The magnetic dissipation $\hat{\mu}(k)$ would not change the equilibrium energy spectrum $\hat{E}(k) \sim k^2$, since it acts equally at all *scalar* wavenumbers k. Therefore, we cannot expect an increase of S if N is increased. The magnetic dissipation does, however, produce a departure from isotropy, and thus from equilibrium, both with respect to the angular energy distribution, and with respect to the energy partition between the components $i = j = n$ and $i = j = p$. The tendency of the nonlinear energy transfer to restore the angular equilibrium has been verified by e.g. Schumann & Herring (1976). This restoration implies an angular (θ) variation of the inertial energy transfer $\hat{\Gamma}_{ii}(\mathbf{k}(\theta))$, which can be measured by

$$S_\theta(t) \equiv \frac{L(t)}{E(t)^{\frac{3}{2}}} \sum_{\text{all } \mathbf{k}} \cos^2\theta \hat{\Gamma}_{ii}(\mathbf{k}, t), \tag{48}$$

with $\cos\theta$ as defined in (27*b*). In the present situation, $\hat{\Gamma}_{ii}(\mathbf{k}(\theta))$ should be

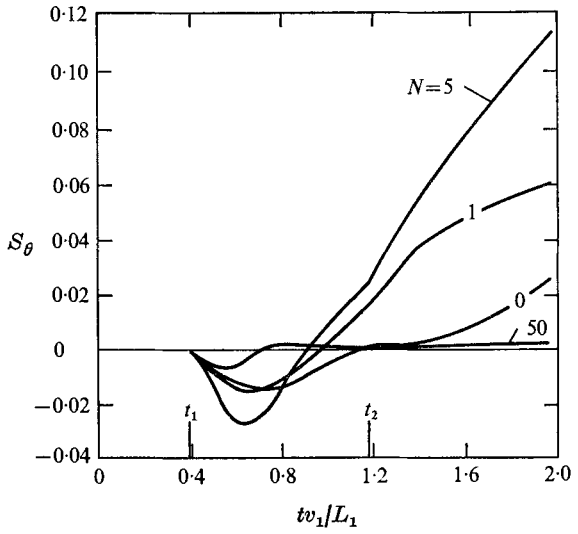

FIGURE 11. Angular 'skewness coefficient' against time.

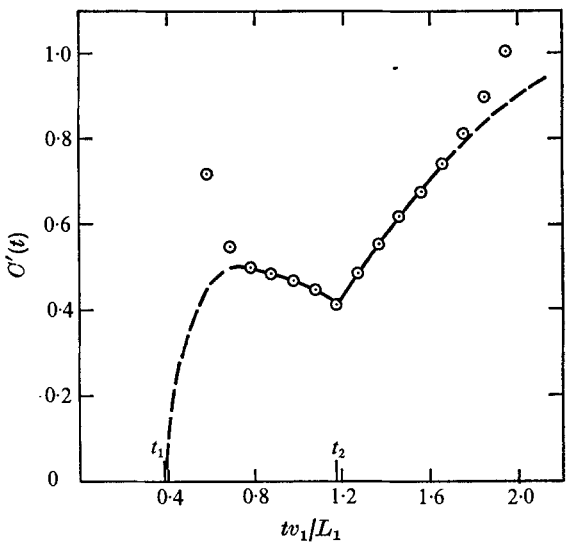

FIGURE 12. Rotta's return rate C' against time for $N = 5$. ⊙, numerical results; – – –, expected function; ——, numerical results.

negative near $\cos^2\theta = 0$ and positive near $\cos^2\theta = 1$; and accordingly we expect a positive value for S_θ. Figure 11 shows the values $S_\theta(t)$ as found numerically. There is a small tendency to negative values initially, which is probably a consequence of initial anisotropies, since it is found even for $N = 0$. Otherwise, we see the expected increase with N for $N = 1, 5$. The result for $N = 50$ shows that, in this case, the magnetic dissipation is strong enough to suppress nearly all angular energy transfer.

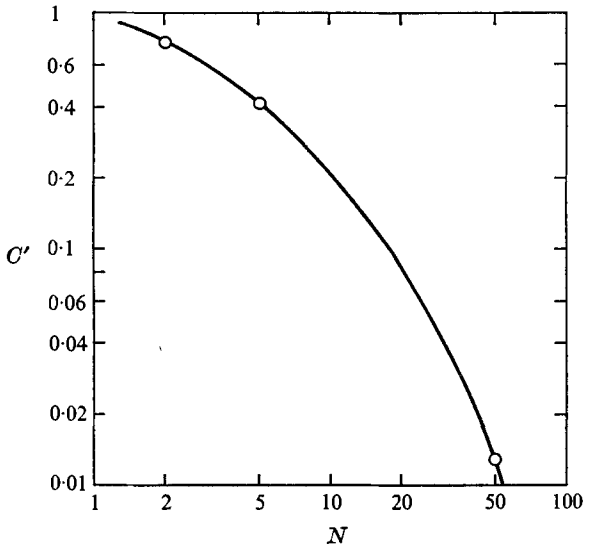

FIGURE 13. Rotta's return rate C' against N. The numerical results are for $N = 2$, 5 and 50 at $t = t_2$.

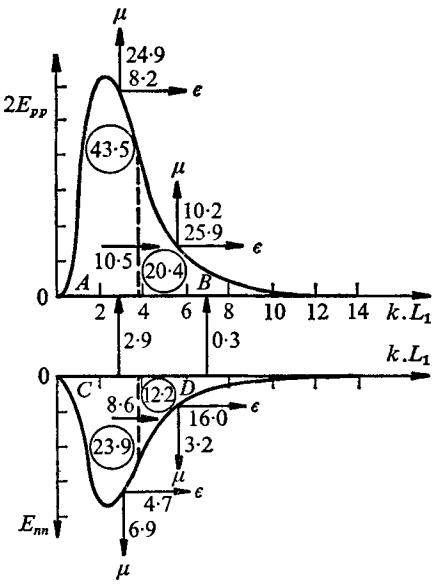

FIGURE 14

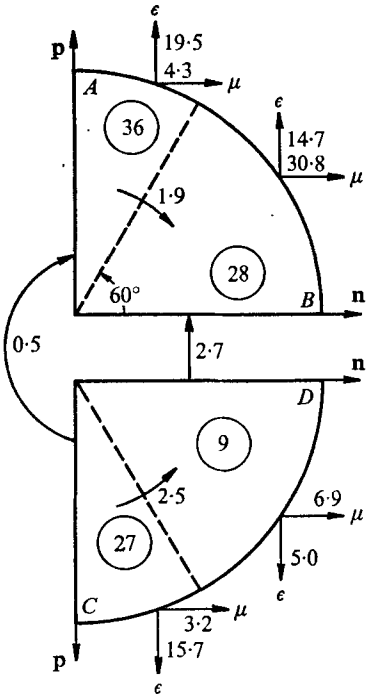

FIGURE 15

FIGURE 14. Energy spectra and energy fluxes in scalar wavenumber space. (See text.) The energy spectra scales are arbitrary. $N = 1$, $t = t_2$.

FIGURE 15. Angular energy distribution and fluxes. (See text.) $N = 1$, $t = t_2$.

The energy exchange between different velocity components and thus between the diagonal components of the energy tensor $\hat{E}_{ij}$ is effected by the nonlinear pressure p_2 as measured by the pressure–strain correlation Φ_{ij}. This has been studied numerically by Schumann & Patterson (1976*b*). The return to isotropy caused by Φ_{ij} can be measured by Rotta's coefficient C', defined in (25). A typical result for $C'(t)$ is shown in figure 12. The numerical results for this coefficient show large statistical errors because of the difference ΔE (see (25)), which is small compared with statistical fluctuations in E_{ij} if the anisotropy is weak (Schumann & Herring 1976). Therefore, we cannot trust the numerical results for $(t-t_1) \ll L_1/v_1$ and $(t-t_2) \gtrsim L_1/v_1$. We see that the magnetic dissipation causes a reduced return-to-isotropy rate. From Schumann & Patterson (1976*b*) and Schumann & Herring (1976), we expect $C' \approx 1$ for $N = 0$. ($C'(t_1) = 0$, because the development of $\Phi_{ij}(t)$ takes a finite time; see Schumann & Patterson (1976*b*). For large values of N, C' is virtually zero. (See figure 13.)

To exemplify the relative importance of these three types of energy transfer ($\hat{\Gamma}_{ii}(k)$, $\hat{\Gamma}_{ii}(\mathbf{k}(\theta))$, Φ_{ij}), we give their values for a specific example ($N = 1, t = t_2$) as a percentage of $(\mu_{ii}+\epsilon_{ii})$ in figures 14 and 15. Figure 14 shows the energy spectra of $\hat{E}_{pp}$ and $\hat{E}_{nn}$. Each spectrum is divided in two regions (A, B and C, D) at $kL_1 = 3{\cdot}79$, which is slightly larger than the wavenumber of the energy peak, but is otherwise arbitrarily chosen. By proper summation of $\hat{\Gamma}_{ij}(\mathbf{k},t)$ over the single regions, we compute the energy flux due to the inertial terms ($A \rightarrow B$ and $C \rightarrow D$), and similarly the flux produced by $p_2(C \rightarrow A,\ D \rightarrow B)$, and by viscous ($\rightarrow \epsilon$) as well as magnetic ($\rightarrow \mu$) dissipation. The actual energy content within the regions is given as a percentage of E_{ii} by the circled numbers. From figure 14 we see that the inertial energy transfer is about one order of magnitude larger than the pressure energy transfer for this situation. Similarly, figure 15 shows the angular energy transfer. The angular regions are separated at $\theta = 60°$, so that the number of modes is equal in both parts. Here, we find that the relative magnitudes of inertial and pressure energy transfer are of comparable size. Both figures 14 and 15 show, however, that the nonlinear energy transfer at this Reynolds number Re_L is one to two orders of magnitude smaller than the dissipation for $N = 1$. This is even more true for greater values of N. We expect, therefore, that the importance of the nonlinear terms is small, for the general flow behaviour, if $N \gg 1$.

4.4. *Comparison of linear with nonlinear results*

Comparing the results obtained for the nonlinear with those obtained for the linear simulations, presented in figures 4–7, 9 and 10, we see several changes caused by the nonlinear terms that are explainable in terms of the energy transfers discussed above. For example, in figure 6, we find a strongly intensified viscous dissipation, which results from the energy transfer from the energy-containing (low) to the dissipating (high) wavenumbers. One would expect a like increase of magnetic dissipation, owing to the angular energy transfer and to that from the **n** components to the **p** components; but the opposite effect can be seen in figure 5. This discrepancy is explained by the fact that the transfer to high wavenumbers is greater than other types of transfer. (See figures 14 and 15.) The nonlinear terms thus result in strong viscous dissipation, which prevents an

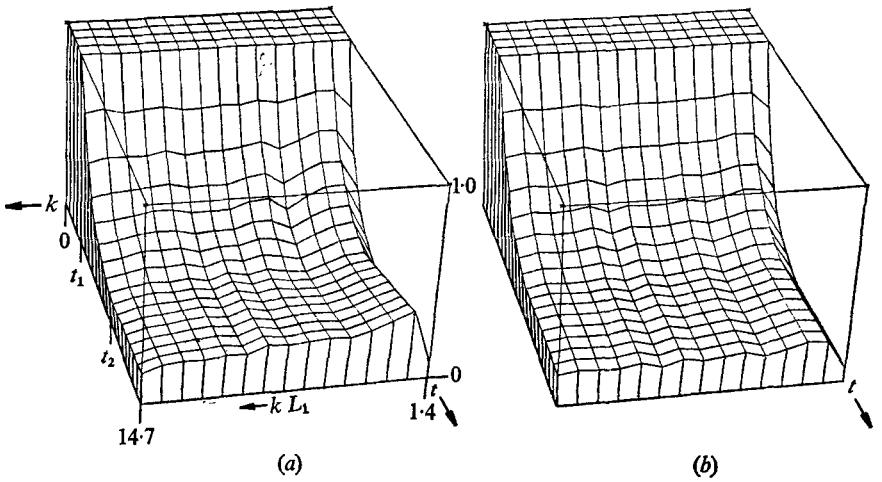

FIGURE 16. Ratio of Hartmann numbers $Ha^2(k, t)/Ha^2(k, t_1)$ against wavenumber k and time t for the nonlinear and linear simulation. (See remark on magnetic field in figure 5.) $N = 5$. (*a*) Nonlinear. (*b*) Linear.

increase of magnetic dissipation. We could expect enhanced magnetic dissipation if the energy spectrum were closer to the equilibrium state and if the Reynolds number Re_L were much larger than it is in these cases. The total dissipation $\epsilon + \mu$ is always larger for nonlinear simulations than for linear ones, as illustrated by the steeper energy decay for nonlinear cases in comparison to the linear results shown in figure 4. The linear simulations exhibit fairly constant values of $Re_\lambda(t)$ and $Re_L(t)$ for $N = 0$ and $t > t_1$ (not plotted); these results are quite different from those obtained for the nonlinear simulations presented in figure 2.

The influence of nonlinear terms is relatively strong with respect to the measures for the two-dimensionality shown in figures 9 and 10. Both figures reflect the return-to-isotropy tendencies produced by the angular inertial energy transfer (figure 9) and by its combination with the pressure energy transfer (figure 10). Additional information is given in figure 16, where the ratio $Ha^2(k,t)/Ha^2(k,t_1)$ is shown in perspective graphs. This ratio is independent of k in the linear approximation and is even insensitive to the inertial energy transfer from low to high wavenumbers k, because such a transfer would change ϵ and μ by the same factor. The nonlinear results do reflect, however, the angular energy transfer. It follows from figure 16 that the latter is greater at high than at low values of k.

Finally, we measure the importance of the nonlinear energy transfer effects by that time t^* for which the difference between the results of the linear simulations and the corresponding results of the nonlinear simulation deviate by 3 % of the latter. The value 3 % is taken arbitrarily, but seems a reasonable value for acceptable errors. This critical time for different results is plotted in figure 17. We see that the shortest critical time appears for the viscous dissipation, which is strongly controlled by the nonlinear terms, independently of N. A longer

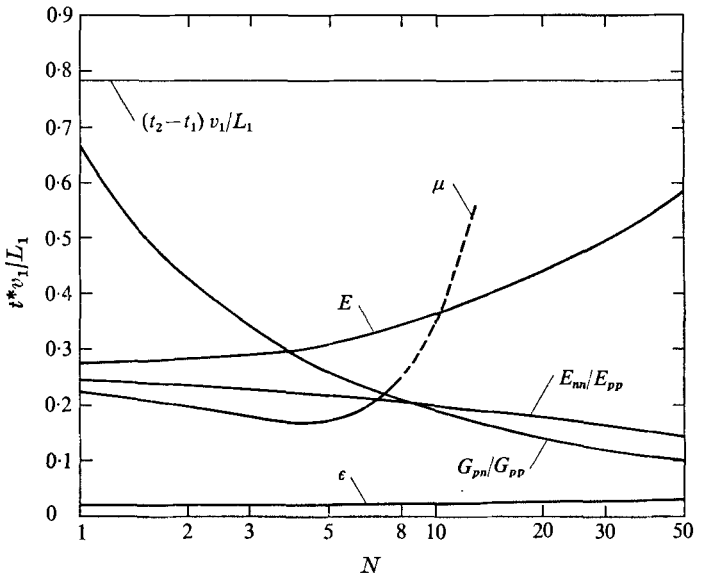

FIGURE 17. Normalized time t^* against magnetic interaction number N for different results; for $t_1 \leqslant t \leqslant t^*$, the differences between the linear and nonlinear results are less than 3 %. Curves are for results with respect to energy E, viscous and magnetic dissipation ϵ and μ and ratios of energies E_{ii} and mean-square gradients $G_{ij} \equiv \langle(\partial u_i/\partial x_j)^2\rangle$ (without summation) for different velocity components.

congruence time t^* is found, especially, for the kinetic energy; the errors with respect to the magnetic dissipation never reached the 3 % level for $N = 50$.

4.5. *Results for the pressure fluctuations*

For r.m.s. values of nonlinear pressure fluctuations, the ratio $\langle p_2^2\rangle^{\frac{1}{2}}/v^2$ was found to be in the range 0·8–1·0 and fairly independent of time *and* of N. So this value stays very close to the results found by Schumann & Patterson (1976*a*) for purely isotropic turbulence. The ratio $\langle p_1^2\rangle^{\frac{1}{2}}/(\sigma B_0^2 vL/\rho)$ is initially about 0·2, as predicted by (43); it approaches zero with increasing values of N. At $t = t_2$ the resultant values are (0·1691, 0·09396, 0·00418) for the nonlinear cases and (0·1697, 0·09993, 0·00358) for the linear simulations with $N = (1, 5, 50)$. At $t = t_1$, the relative contribution $\langle p_1^2\rangle^{\frac{1}{2}}/\langle p_1^2+p_2^2\rangle^{\frac{1}{2}}$ of the linear pressure fluctuations to the total pressure fluctuations is (0·17, 0·65, 0·99) for $N = (1, 5, 50)$. These numbers even grow slightly with time during (t_1, t_2); thus, for $N = 50$, more than 99 % of the pressure fluctuations are caused by the Lorentz force. These fluctuations are concentrated at rather small wavenumbers. (See (39).)

The ratio $3\mu_{23}/\mu_{kk}$ should vary between 0·6 (refer to (37)) and 0·5, from the linear theory. The ratio controls the parameter C_F, and thus the linear pressure energy transfer ϕ_{ij}. The results show mean values of the order of 0·6, but they also show relatively strong fluctuations, that are probably a consequence of deviations from isotropy in the initial state. The nonlinear pressure energy transfer, measured in terms of C', has been discussed above.

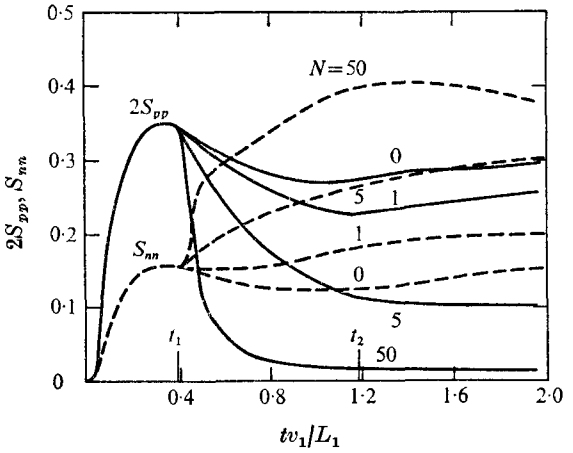

FIGURE 18. Skewness coefficients S_{pp} and S_{nn} against time.

4.6. *Two-dimensional aspects*

Two-dimensional turbulence differs essentially from three-dimensional turbulence (Kit & Tsinober 1971; Leith 1968; Lilly 1971; Herring *et al.* 1974; Pleshanov & Tseskis 1973). In two dimensions, enstrophy (which is $\epsilon/(2\nu)$) cannot be created by nonlinear effects, only destroyed by viscosity, implying zero integral enstrophy transfer $\Sigma\, k^2 \hat{\Gamma}_{ii}(\mathbf{k}, t)$. Thus the skewness coefficient $S(t)$, defined in (25), should go to zero when we approach the two-dimensional state. However, this is contrary to the results shown in figure 3. We find that the skewness stays nearly independent of time and of N. Closer inspection of the contributions of the single components $\hat{\Gamma}_{ij}(\mathbf{k}, t)$ to S shows that the invariance of S with N is the result of two counteracting effects. Figure 18 shows the two skewness coefficients S_{pp} and S_{nn},

$$\left.\begin{aligned} S_{nn} \equiv S_{33}, \quad S_{pp} \equiv \tfrac{1}{2}(S_{11}+S_{22}), \\ S_{ij} \equiv \tfrac{1}{35}[15\nu/\epsilon]^{\frac{3}{2}} \Sigma\, \hat{\Gamma}_{ij}(\mathbf{k}, t) k^2, \end{aligned}\right\} \tag{49}$$

where the sum is taken over all wavenumbers $\mathbf{k}$. The definitions are such that $S = S_{nn} + 2S_{pp}$. We find that $S_{pp}(t)$ goes to zero with increasing N. At the same time, $S_{nn}(t)$ increases with N, however, so that S remains about constant. The conclusion is that, for a quasi-two-dimensional turbulent flow, the velocity components in the plane $\mathbf{k}.\mathbf{n} = 0$ behave as expected from two-dimensional turbulence theories; but the normal component does not. In the limit to pure two-dimensionality, the Navier–Stokes component for u_n reduces to that for a scalar quantity, since

$$\partial u_n/\partial x_n = \partial p/\partial x_n = 0,$$

and its transport towards high wavenumbers is non-zero. A consequence of this result is demonstrated by figure 19, which shows the ratio $\hat{E}_{nn}(k, t)/\hat{E}_{pp}(k, t)$. In the linear approximation with isotropic initial conditions, the latter cannot become larger than two, as found in (31). The nonlinear results show, however, a peak value of (1·41, 1·82, 3·71, 11·3) for $N = (1, 2, 5, 50)$ at $t = t_2$. On the other hand, this ratio is decreased by the nonlinear terms at low wavenumbers.

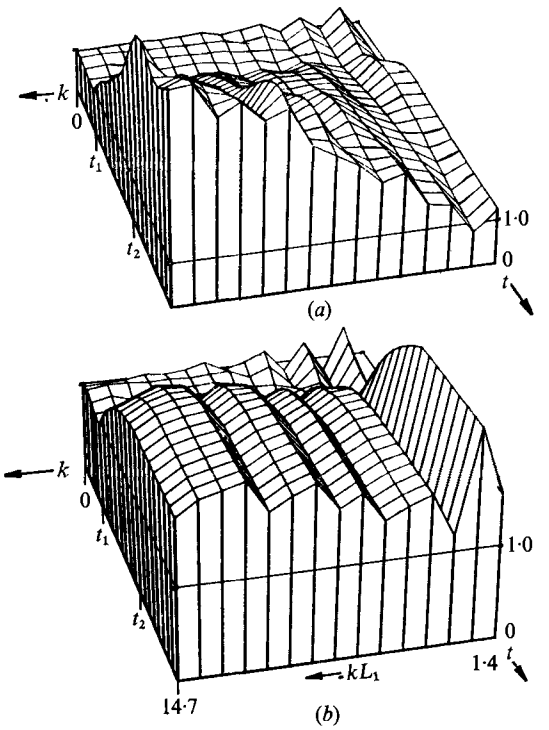

FIGURE 19. Energy ratio $\hat{E}_{nn}(k, t)/\hat{E}_{pp}(k, t)$ against wavenumber k and time t. $N = 5$. (*a*) Nonlinear. (*b*) Linear.

Another property of two-dimensional turbulence is that energy is transported partly from moderate to low wavenumbers, and thus increases the integral length scale L. This property is reflected by the results for $Re_L(t)$ shown in figure 2; the Reynolds number becomes larger for $N = 50$ than for $N = 5$, after some time.

Finally, we report some results that characterize the final two-dimensional state at $t = t_2$ for $N = 50$. For this purpose, we compute all statistics for the $\mathbf{p}$ components with $\mathbf{k}.\mathbf{n} = 0$ only. For the integral and micro-Reynolds numbers R_L and R_l and for the two-dimensional skewness S_2, we find the values $R_L = 7{\cdot}3$, $R_l = 1{\cdot}34$ and $S_2 = 0{\cdot}24$. These quantities have been defined by Herring *et al.* (1974), using the same nomenclature. The skewness S_2 is a measure of the enstrophy transport from low to high wavenumbers and proportional to $\Sigma k^4 \hat{\Gamma}_{ii}(\mathbf{k}, t)$. We see that the Reynolds numbers are much smaller than those reached by Herring *et al.* (1974), a consequence of the smaller resolution of this plane. Whereas in Herring *et al.* (1974) an 128×128 grid was used, the present results correspond to only a 32×32 grid. In view of the much smaller resolution and Reynolds number, the present result $S_2 = 0{\cdot}24$ is not too far away from the result $S_2 \approx 0{\cdot}4$ in Herring *et al.* (1974). The general behaviour of $S_2(t)$ is plotted in figure 20, which shows that S_2 is much larger when the modes $\hat{\mathbf{u}}(\mathbf{k}, t)$ at $\mathbf{k}.\mathbf{n} \neq 0$ are not all zero.

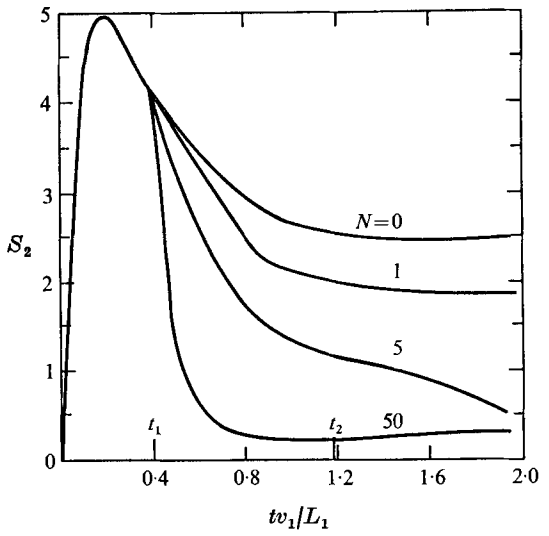

FIGURE 20. Two-dimensional skewness coefficient S_2 as defined by Herring *et al.* (1974) against time.

4.7. *Critical interaction and Reynolds numbers*

We are looking for an estimate for that critical value N_c of N for which the magnetic dissipation is strong enough to prevent a return from the two-dimensional to the three-dimensional state. For this purpose we determine the minimum value of $\sigma B_0^2(t)/\rho$ that makes $d\hat{E}_{ij}(\mathbf{k},t)/dt$ zero or negative for all $\mathbf{k}$ with $\mathbf{k}.\mathbf{n} \neq 0$. This value is found from (23), (24) by use of the computed results for $\hat{E}_{ij}$, $\hat{\Gamma}_{ij}$, $\hat{\Phi}_{ij}$ and $\hat{e}_{ij}(\mathbf{k},t)$. Because these values are determined from the velocity field by averaging over rings around the axis of symmetry $\mathbf{n}$ only, the results exhibit large statistical errors. The values

$$N_c(t) = \sigma B_0^2(t) L_1/(\rho v_1)$$

are presented in figure 21. Figure 22 contains similar results for the minimum viscosity $\nu_c(t)$ or for the critical Reynolds number

$$Re_c(t) = v_1 L_1/\nu_c(t).$$

The results show a steady decrease of N_c and Re_c^{-1} for $N = 0, 1, 5$, and against time, as a consequence of the damped nonlinear terms. Some anomalies are found for $N = 50$. Here we get a very large critical value Re_c^{-1} if we consider the component $\hat{E}_{nn}(\mathbf{k},t)$ alone, whereas that for the $\mathbf{p}$ components is much smaller. This again is a consequence of the large energy transfer for the $\mathbf{n}$ component. The differences between the $\mathbf{n}$ and $\mathbf{p}$ components have been found to be within the statistical uncertainties with respect to N_c. However, the value N_c is significantly larger in this case than for $N = 1$ and 5, especially near $t = t_2$. So the instability of the resultant quasi-two-dimensional state increases when we approach pure two-dimensionality. Typical results are $N_c \approx 50$, $Re_c \approx 30$.

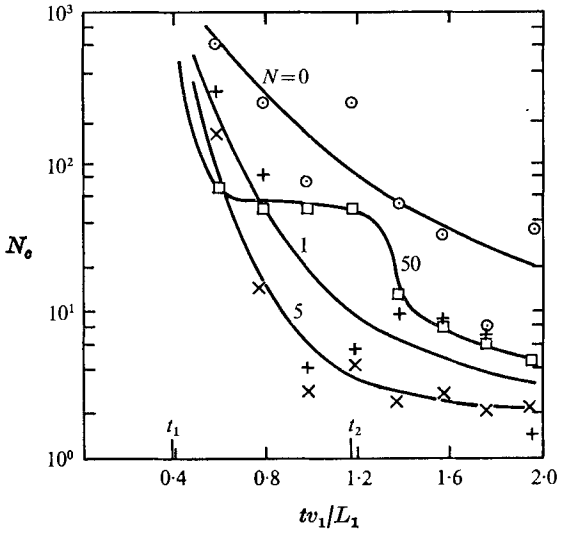

FIGURE 21. Critical magnetic interaction number N_c against time. Numerical results are represented by the different points. Curves are estimated fits.

N: ⊙, 0; +, 1; ×, 5; □, 50.

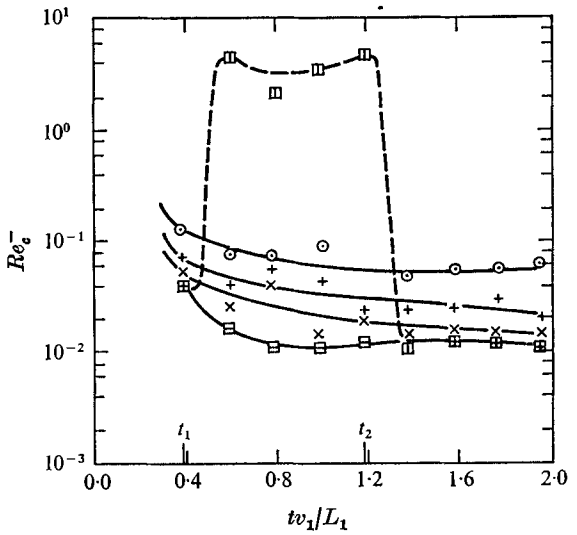

FIGURE 22. Critical normalized viscosity $\nu_c = Re_c^{-1}$ against time. The points and curves are as in figure 21. For $N = 50$ the results are shown for the **n** and **p** components separately.

N	0	1	5	50	
				n	**p**
	⊙	+	×	⊞	⊟

5. Concluding discussion

The transition from three- to two-dimensional turbulence under a uniform magnetic field has been simulated numerically. The direct spectral simulation method of Orszag & Patterson (1972) has been found to be applicable for this case. Since the transition is best understood in wavenumber space, this scheme seems to be more appropriate than e.g. a finite-difference simulation in real space. Also, the spectral method gives exact results with respect to the linear evolution for the given boundary conditions. The discrete resolution in wavenumber space implied by the finite box size, however, introduces important departures from continuum behaviour. One could, perhaps, design a spectral code with varying values of the box side lengths in different directions, and as a function of the turbulence evolution; but this would require drastic changes in the method, and has accordingly not been elaborated.

The finite resolution would be also a problem if analytical turbulence theories were used. Schumann & Herring (1976) showed for the direct-interaction approximation of Kraichnan (1964) and Herring (1974) that the description of angular anisotropy is an important problem of the numerical procedure that describes the angular variation in terms of a few Legendre moments. For the present case with statistically unidirectional forces (and also in other similar situations, such as those in which buoyancy forces occur), the results of Schumann & Herring (1976) are even more striking. One could perhaps resolve that difficulty in this special case, using the linear solution (22), and describing only departures from it in terms of Legendre moments.

The linear results are as expected from linearized theories. We stressed the different kinds of anisotropies and the resultant pressure fluctuations. In particular, we found highly intensified pressure fluctuations, and deduced a relationship for the pressure–strain correlation resulting from the Lorentz force (equation (36)).

The nonlinear simulations show that the linear theories are applicable (within 3 % error) for times $(t-t_1) \leqslant \gamma L_1/v_1$ (as suggested by Moffatt 1967). The factor γ is of the order 0·2 and, thus, smaller than estimated earlier (Moffatt 1967); it is, however, dependent on the quantity one is interested in, and on the value of the interaction number N as shown in figure 17. The nonlinear terms produce energy transfer from low to high wavenumbers, angularly out of the plane $\mathbf{k}.\mathbf{n} = 0$ into the region near the axis $\mathbf{n}$, and between the different velocity components. The first transfer is usually much larger than the two others, especially when we reach the quasi-two-dimensional state. In the latter situation, there is also some energy transfer towards low wavenumbers, but only with respect to the velocity components in the plane $\mathbf{k}.\mathbf{n} = 0$. In spite of these nonlinear energy transfers, the magnetic dissipation can be strong enough to cause at least a quasi-two-dimensional state; a purely two-dimensional state does not seem to be possible for decaying turbulence. The size of the critical interaction number N_c is of the order of 50. This result stems from a rather crude stability analysis; N_c is certainly dependent on Re_L and possibly on other parameters. From the nonlinear results, we find that the anisotropies introduced by the magnetic field are not negligible

even for $N = 1$. The value $N_{\min}$ below which they are sufficiently small can be estimated to be of the order of 10^{-2}.

Perhaps the most surprising result is the behaviour of the skewness coefficient S, which is a measure for that energy transfer which increases the viscous dissipation rate. This coefficient was expected to go to zero, but for quasi-two-dimensional turbulence it was found to stay fairly constant. (See figure 3.) In fact, the nonlinear transport of energy $\hat{E}_{nn}$ of the velocity component normal to the plane $\mathbf{k}.\mathbf{n} = 0$ becomes much larger than that of the components ($\hat{E}_{pp}$) in the plane of the final two-dimensionality. (See figure 19.) This result is relevant to turbulence models for the atmosphere: large-scale atmospheric turbulence is like the quasi-two-dimensional state we study here. The invariance of the total skewness suggests that atmospheric turbulence is perhaps better described in terms of three-dimensional than two-dimensional turbulence models.

The magnetic dissipation is large compared with the viscous dissipation only in the energy-containing region. Moreover, the nonlinear transport effects that cause a return to isotropy are large at high wavenumbers. We might, therefore, use the subgrid scale model approach (Schumann 1975) to extend the present results to higher Reynolds numbers Re_L. In this approach, only the energy-containing scales are simulated directly, and turbulence models are used to describe the fine-scale turbulence, which cannot be resolved on our present computers. In a first approximation, these models do not even have to account for the anisotropies introduced by the magnetic field, at least for $N \lesssim 5$. This approach would allow investigation of the changes in friction and heat transfer in channel flows caused by the uniform magnetic field.

This paper was presented at the Twelfth Biennial Fluid Dynamics Symposium on Advanced Problems and Methods, 8–13 September 1975, Bialowieza, Poland. The work was done while the author was on leave with the Advanced Study Program of the National Center for Atmospheric Research, Boulder, Colorado, which is sponsored by the National Science Foundation.

REFERENCES

BATCHELOR, G. K. 1959 *The Theory of Homogeneous Turbulence*. Cambridge University Press.

HERRING, J. R. 1974 Approach of axisymmetric turbulence to isotropy. *Phys. Fluids*, **17**, 859–872.

HERRING, J. R., ORSZAG, S. A., KRAICHNAN, R. H. & FOX, D. G. 1974 Decay of two-dimensional homogeneous turbulence. *J. Fluid Mech.* **66**, 417–444.

KIT, L. G. & TSINOBER, A. B. 1971 Possibility of creating and investigating two-dimensional turbulence in a strong magnetic field. *Magn. Girodin.* **7**, 27–34.

KRAICHNAN, R. H. 1964 Decay of isotropic turbulence in the direct interaction approximation. *Phys. Fluids*, **7**, 1030–1048.

LAUNDER, B. E. 1975 On the effects of a gravitational field on the turbulent transport of heat and momentum. *J. Fluid Mech.* **67**, 569–581.

LEHNERT, B. 1955 The decay of magneto-turbulence in the presence of a magnetic field and Coriolis force. *Quart. Appl. Math.* **12**, 321–341.

LEITH, C. E. 1968 Two-dimensional eddy viscosity coefficients. *Proc. WMO-IUGG Symp. on Numerical Weather Prediction, Tokyo*, vol. 1, pp. 1–44.

LILLY, D. K. 1965 On the computational stability of numerical solutions of time-dependent nonlinear geophysical fluid dynamics problems. *Mon. Wea. Rev.* **93**, 11–26.

LILLY, D. K. 1971 Numerical simulation of developing and decaying two-dimensional turbulence. *J. Fluid Mech.* **45**, 395–415.

MOFFATT, H. K. 1967 On the suppression of turbulence by a uniform magnetic field. *J. Fluid Mech.* **28**, 571–592.

MOREAU, R. 1968 On magnetohydrodynamic turbulence. *Proc. Symp. on Turbulence of Fluids and Plasmas, Polytechnic Institute of Brooklyn*, pp. 359–372.

ORSZAG, S. A. & PATTERSON, G. S. 1972 Numerical simulation of three-dimensional homogeneous isotropic turbulence. *Phys. Rev. Lett.* **28**, 76–79.

PLESHANOV, A. S. & TSESKIS, A. L. 1973 Two-dimensional turbulence in a magnetic field. *Magn. Girodin.* **9**, 137–139.

POUQUET, A. & PATTERSON, G. S. 1976 Numerical simulation of helical magnetohydrodynamics turbulence. Submitted to *J. Fluid Mech.*

REYNOLDS, W. C. 1973 Recent advances in the computation of turbulent flows. *Adv. in Chem. Engng* **9**, 193–246.

ROBERTS, P. H. 1967 *An Introduction to Magnetohydrodynamics*. New York: American Elsevier.

ROTTA, J. 1951 Statistische Theorie nichthomogener Turbulenz. *Z. Phys.* **129**, 547–572.

SCHUMANN, U. 1975 Subgrid scale model for finite difference simulations of turbulent flows in plane channels and annuli. *J. Comp. Phys.* **18**, 376–404.

SCHUMANN, U. & HERRING, J. R. 1976 Axisymmetric homogeneous turbulence: a comparison of direct spectral simulations with the direct interaction approximation. Submitted to *J. Fluid Mech.*

SCHUMANN, U. & PATTERSON, G. S. 1976*a* Numerical study of pressure and velocity fluctuations in nearly isotropic turbulence. Submitted to *J. Fluid Mech.*

SCHUMANN, U. & PATTERSON, G. S. 1976*b* Numerical study of the return of axisymmetric turbulence to isotropy. Submitted to *J. Fluid Mech.*

VOLKOV, A. V. 1973 The effects of a magnetic field on the turbulence behind a grating *Magn. Girodin.* **9**, 26–32.